RESEARCH ARTICLE | MARCH 31 2008

Exciton quenching in emitter blends for organic light emitting devices probed by electric field–dependent time-resolved luminescence

J. Kalinowski; J. Mężyk; F. Meinardi; R. Tubino; M. Cocchi; D. Virgili

J. Chem. Phys. 128, 124712 (2008)
https://doi.org/10.1063/1.2841458

Exciton quenching in emitter blends for organic light emitting devices probed by electric field–dependent time-resolved luminescence

J. Kalinowski,[1,a] J. Mężyk,[2] F. Meinardi,[2] R. Tubino,[2] M. Cocchi,[3] and D. Virgili[3]
[1]*Department of Molecular Physics, Gdańsk University of Technology, ul. G. Narutowicza 11/12, 80-952 Gdańsk, Poland*
[2]*Department of Material Sciences, University of Milan Bicocca, via R. Cozzi 53, 1-20125 Milano, Italy*
[3]*Institute of Organic Synthesis and Photoreactivity, National Research Council of Italy, via P. Gobetti 101, 1-40129 Bologna, Italy*

(Received 8 October 2007; accepted 15 January 2008; published online 31 March 2008)

We investigate quenching mechanisms of excited states in emitter layers for organic light emitting diodes (LEDs). An extensive study of a strong electric field–induced modulation (over 50%) of the time-resolved luminescence in a diamine derivative (TPD): polycarbonate blend films doped with an organic complex of europium are presented as a typical example of an important class of emitters for organic monochromatic LEDs. Using this method allowed us to identify the quenched species as the excited ligand precursors of the emissive europium ion states. Manipulating the electrode materials and their electrical bias, the electric field–enhanced dissociation, and interaction with injected charge could be separated and found as principal quenching mechanisms. We show the first one to follow the three-dimensional Onsager theory of geminate recombination, and the second one raised by their interaction with the TPD-transported holes. The interaction rate constant is found to be underlain by the three-dimensional diffusion of excited ligand singlets, combining the exciton diffusion coefficient and long-range (Förster type) energy transfer parameters. The dynamic parameters of the hole-precursor excitons interactions, extracted from the experimental data, allow us to establish the criteria for identifying useful ligands and matrices in the optimized design of electrophosphorescent, linelike emitting molecules, and device structure for organic LEDs. © *2008 American Institute of Physics*. [DOI: 10.1063/1.2841458]

I. INTRODUCTION

A strong roll off in the quantum efficiency observed in organic LEDs operated at high electric fields (large current densities)[1–7] is one of the most important factors limiting their performance. The roll off is thought to be a result of at least three processes quenching the excited states: (i) exciton-exciton annihilation,[4,6] (ii) exciton charge carrier interaction,[4,7] and (iii) electric field–induced exciton dissociation.[1,3,7] Clearly, a combination of all these quenching mechanisms determines optical performance of organic LEDs at high electric fields. Thus, attempts to explain high field emission characteristics of organic LEDs basing on one of them only would fail or present a crude approximation at most of complex processes underlying their function. Previously, exciton-exciton interactions have been separately examined by measurements of the photoluminescence (PL) response to increasing excitation intensity.[8–10] The measurement of PL quenching at low excitation intensities in films sandwiched between two electrodes allowing the application of external voltage would provide the missing link in order to disentangle bimolecular exciton-exciton interactions and electric field effects on exciton behavior. However, from steady-state PL quenching studies in films provided with charge injecting electrodes one cannot decide if excitons are quenched by mechanism (ii) or (iii). Recently, organic thin film electroluminescence (EL) emitters provided with weakly injecting low-work function electrodes (Al/emitter/Al) have been studied in order to eliminate mechanism (ii).[11–13] The results, though generally plausible, do not resolve an important issue of the quenching mechanisms. In particular, the nature of quenched species remains an open question. Among a variety of emitters for LEDs, those based on europium chelates are of particular interest and importance since their narrow-band (linelike) emission spectra in the red appear suitable to manufacture pure red and full color EL devices.[1–3,14–16] In these emitters both PL and EL, originate from $^5D_0 \rightarrow {}^7F_n$ $(n=0,1,\ldots,6)$ transitions of the Eu^{3+} ion, its excited states being populated by the energy transfer from excited organic ligands. The ligands are excited either by direct absorption of light[16] or by the recombination on them of electrons and holes injected initially at electrical contacts.[6] They can also be populated by energy transfer from other molecules for Eu complex dispersed in an organic matrix[4,6] as usually is the case with organic LEDs.

We are mainly concerned in this work with a question whether the emissive Eu^{3+} ion excited states or their precursors are affected by charge injected at the electrodes and what is the mechanism of their dissociation enhancement by the applied electric field. In the time-resolved measurements, amplitude quenching and lifetime quenching are possible to distinguish.[17] In amplitude quenching only the precursor of the emissive state is quenched. Alternatively, in the lifetime

[a]Author to whom the correspondence should be addressed. Electronic mail: kalino@polnet.cc.

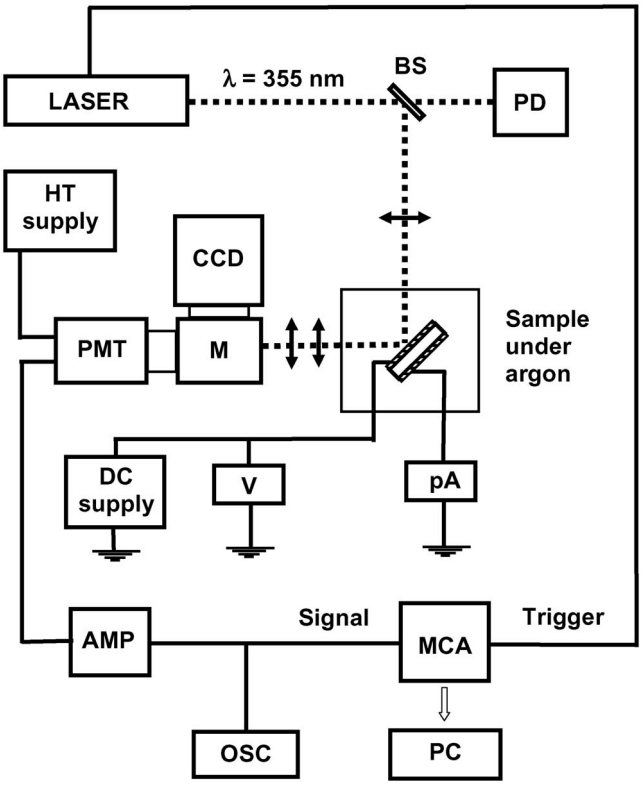

FIG. 1. The experimental setup for the electric field-modulated time-resolved PL measurements. The setup consists of laser-Nd: YAG laser as a source of excitation producing 10 ns duration pulses of light ($\lambda = 355$ nm) with the repetition rate tunable between 200 Hz and 10 kHz, PD: photodiode to control the average excitation intensity, BS: beam splitter, M: monochromator, PMT: photomultiplier tube, AMP: amplifier, OSC: oscilloscope, and MCA: multichannel analyzer. The sandwich configuration samples were excited through the glass substrate and indium-tin-oxide (ITO) layer. Electric field applied to the sample originated from a dc supply being controlled by a voltmeter (V). The current flow through the sample was controlled by a picoammeter (pA). All measurements were performed at room temperature under argon atmosphere.

quenching only the emissive state is quenched. We will use the time-resolved PL to elucidate the processes responsible for the mechanism of PL quenching in Eu complex-doped blend films composed of a diamine derivative (TPD) and polycarbonate (PC), manipulating the material and bias of the electrodes that allow either the application of an electric field or electric field combined with efficient charge injection into the film samples. The results are of essential importance particularly for understanding the function of linelike emitting, europium chelates-based LEDs and more generally for organic device physics.

II. EXPERIMENTAL METHOD

The PL quenching was studied on the front $h\nu_{\mathrm{exc}} \rightarrow$glass/indium-tin-oxide (ITO) face excited ($h\nu_{\mathrm{exc}}$) sandwich film structures $h\nu_{\mathrm{exc}} \rightarrow$glass/ITO/6 wt %Eu1: 74%TPD:20%PC (200–250 nm)/Au or Al; the emission being recorded from the illuminated glass/ITO side. The sample configuration and the experimental setup are shown in Fig. 1. The Eu1 stands for a short designation used in this work for the Eu organic complex of tris(di(bromo)benzoylmethane)mono(phenathroline) europium (III), the compound purchased from SANDS Corp. and used as supplied. The Eu1 was doped into blend films composed typically of 74% of *N*,*N*′-diphenyl-*N*,*N*′-bis(3-methylphenyl)-[1,1′-biphenyl]-4,4′-diamine (TPD) and 20% of bisphenol-A-polycarbonate (PC). The hole transporting TPD was purchased from Aldrich and electronically neutral PC of molecular weight of 32 000–36 000 from Polysciences Inc., both used as supplied. Samples were cast using spin coating technique from a 10 mg/ml dichloromethane solution onto patterned precleaned transparent to visible light ITO coated glass substrates (20 Ω/sq), then covered by vacuum evaporation with either gold or aluminum. Typically, the electrically active sample areas were about 7 mm^2. Measurements were performed in an argon atmosphere at room temperature on Eu1-doped TPD:PC blend samples illuminated at 355 nm. The method is based on time-correlated photon counting (see Fig. 1). For 355 nm illumination a Nd:YAG (yttrium aluminum garnet) laser was used producing 10 ns duration time pulses of UV light with the repetition rate tunable between 200 Hz and 10 kHz. Typical excitation densities were 10–100 $\mathrm{nJ/cm}^2$ with the laser spot size of ≈0.1 cm, which corresponds to the quantal flux range of 8×10^{13}–8×10^{14} photons/cm^2 s. Taking into account the optical density of the blend films at 355 nm and individual pulse energy E_{pulse}, we estimated that the average concentration $(0.63E_{\mathrm{pulse}}/V_{\mathrm{exc}}h\nu_{\mathrm{exc}})$ of excitons is active in the sample volume $V_{\mathrm{exc}}=S_{\mathrm{laser}}\times l_a$, where S_{laser} is the laser beam spot area and l_a is the penetration depth of the exciting light. Thus, of the excitation intensity I_0 a fraction $I(l_a)/I_0=1-\exp(-\alpha l_a)$ ≈63% remains within the penetration depth ($l_a=\alpha^{-1}$) of the exciting light. This is a reasonable approximation assuming the incident light to be absorbed predominantly by the TPD component of the blend samples within the volume V_{exc}, the rest of the sample does not contribute noticeably to the measured data. It is accounted for in the quantitative fit of the experimental data to theory, a fraction of 0.63 can be found in Eqs. (5) and (6).

The absorption (ABS) and PL spectra of Eu1 as shown in Fig. 2 are in accordance with earlier results.[12] The PL at 612 nm was monitored by a charge coupled device Spex light detector and a Philips 150 CVP photomultiplier tube (PMT). Photon counts from the PMT were processed by an ORTEC 9353 system and accumulated by a personal computer. Data were taken with a maximum resolution of 100 ps/channel. The total excitation intensity was controlled with an Ophir Optronics Ltd. PD300-UV-SH photodiode (PD). Signals are collected in the presence and absence of electric fields produced by a steady-state variable voltage bias applied to the electrodes. Different decay curves were collected for every applied field corresponding to positive, negative, and zero ITO electrode bias.

III. EXPERIMENTAL RESULTS

In Fig. 3 the PL decay curves for Eu1-doped PC and TPD:PC films on glass substrates are presented with 355 nm excitation and PL measured at 612 nm. For both measurements the nonexponential decay is observed. Its rough single

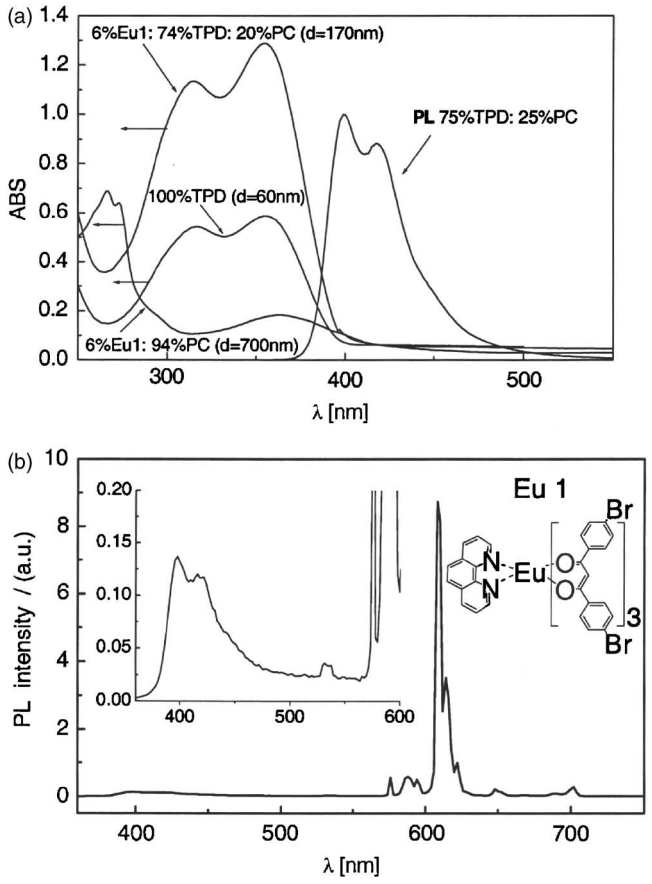

FIG. 2. Absorption (a) and photoluminescence (PL) (b) spectra of an Eul-doped (TPD:PC) films. The absorption spectra of a 100% TPD and PL spectrum of (75%TPD:25%PC) films are shown for comparison [plot (a)]. The PL spectrum taken for a 6 wt %Eul:74%TPD:20%PC(215 nm) does not differ from that for a 6 wt %Eul:94%PC (350 nm) in the wavelength region above 550 nm, but the short-wavelength (350–550 nm) features can be observed in the former [see the inset in plot (b)] and ascribed to the emission of TPD combined possibly with the emission of ligands and bimolecular excited states.

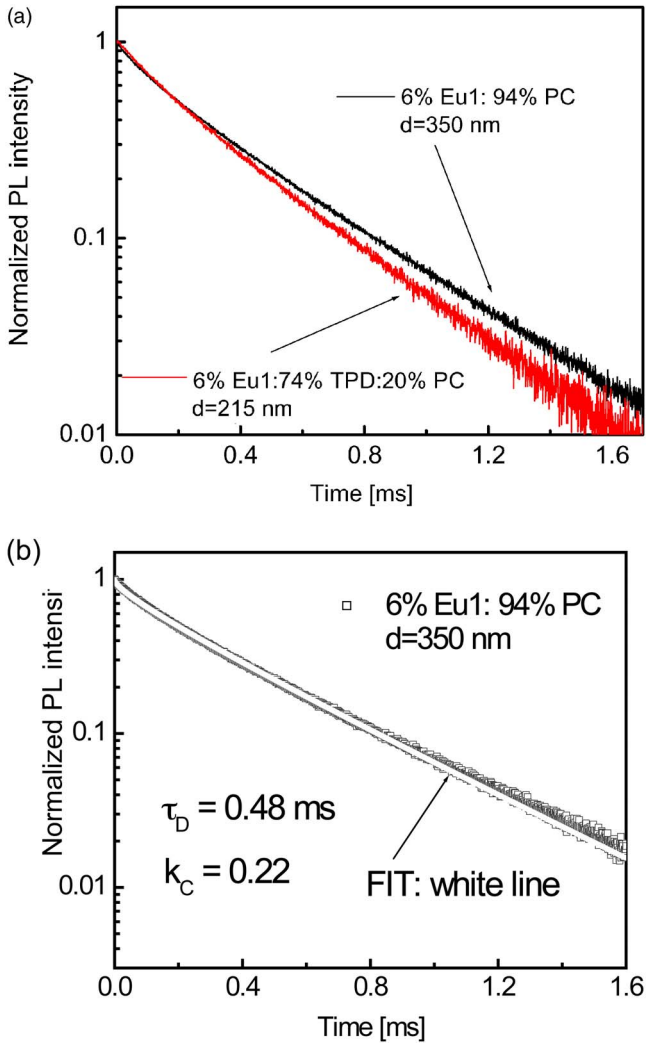

FIG. 3. (Color online) PL decay curves for Eul-doped films as indicated in the figure. A slightly faster decay is observed for the (TPD:PC) blend than for pure PC matrix (a). The experimental data (squares) can well be approximated by Eq. (1) (white line) with τ_D and k_c given in part (b) of the figure. Time-resolved luminescence was measured at 355 nm excitation and 612 nm detection.

exponential approximation allows us to estimate the apparent decay time for the first TPD devoid sample on $\tau = 360 \pm 4$ μs, which is slightly longer than that, $\tau = 315 \pm 3$ μs, for the TPD:PC blend sample. Such defined parameter τ is sufficient to qualitative compare the temporal behavior of these two different film structures. In a more exact analysis, we assign the observed nonexponential decay to a long-range (dipole-dipole coupling) energy transfer from excited Eu^{3+} states (energy donors D) to less efficiency emitting and/or nonemissive species (energy acceptors A), the latter being most probably dopant aggregates formed efficiently in PC and PC:TPD blends.[11,12] The decay of excited Eu^{3+} ions accounted for such an energy transfer process is given by[18]

$$\Phi(t) = \Phi(0)\exp\{-[t/\tau_D + 2k_c(t/\tau_D)^{0.5}]\}, \quad (1)$$

where $\Phi(0)$ is the PL intensity amplitude, τ_D the donor emission lifetime at zero acceptor concentration c (moles/liter), and $k_c = c/c_0$ with $c_0 = 3 \times 10^3 / 2\pi N R_0^3$ corresponding to the Förster radius R_0 (cm), and N standing for Avogadro's number. A satisfactory fit to experimental decays can be achieved with function (1) [Fig. 3(b)]. The effect of the nonhomogeneous dopant environment shows up also in a reduction of the effective lifetime of its excited states when films are sandwiched between ITO and metal layers [Fig. 4(a)]. Clearly, exciton quenching at the ITO and metal contacts underly the observed reduction of the lifetimes. As comes out from the absorption spectra presented in Fig. 2, molecular singlet excitons of TPD are primarily excited states produced in the major part within the penetration depth of the exciting light $l_a < 60$ nm within the 350–355 nm range. Thus, the interface quenching effect on the emissive states within the penetration depth region is not surprising. The quenching mechanism is likely due to the long-range energy transfer and/or short-range charge transfer to the metal (semiconductor) contact.[1,19,20] The quenching on chemical and/or physical defects created locally during contact formation cannot be excluded though.[21] A possible role of the second order exciton-exciton interactions in the generation of the nonexponential decay of the PL can be ruled out since the curvature of the decay curve appears to be independent of the

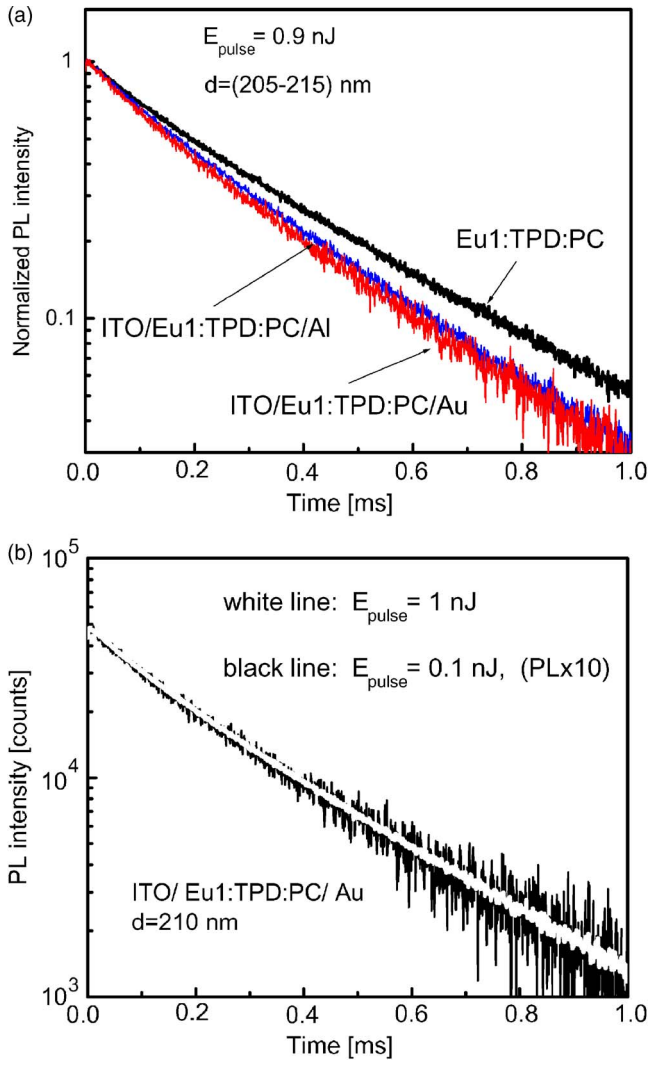

FIG. 4. (Color online) (a) Time-resolved luminescence measured at 355 nm excitation and 612 nm detection for Eul-doped samples with different metal contacts (Al, Au) as compared with that for a glass-deposited film of Eul: TPD:PC. (b) Normalized PL decays for a 210-nm-thick Eul-doped (TPD:PC) film, sandwiched between ITO and Au layers, at different excitation intensities as indicated in the figure. No difference is detected in their curvature at low (white line) and a ten times stronger excitation (black line). Excitation and detection wavelengths as previously in Figs. 1 and 2.

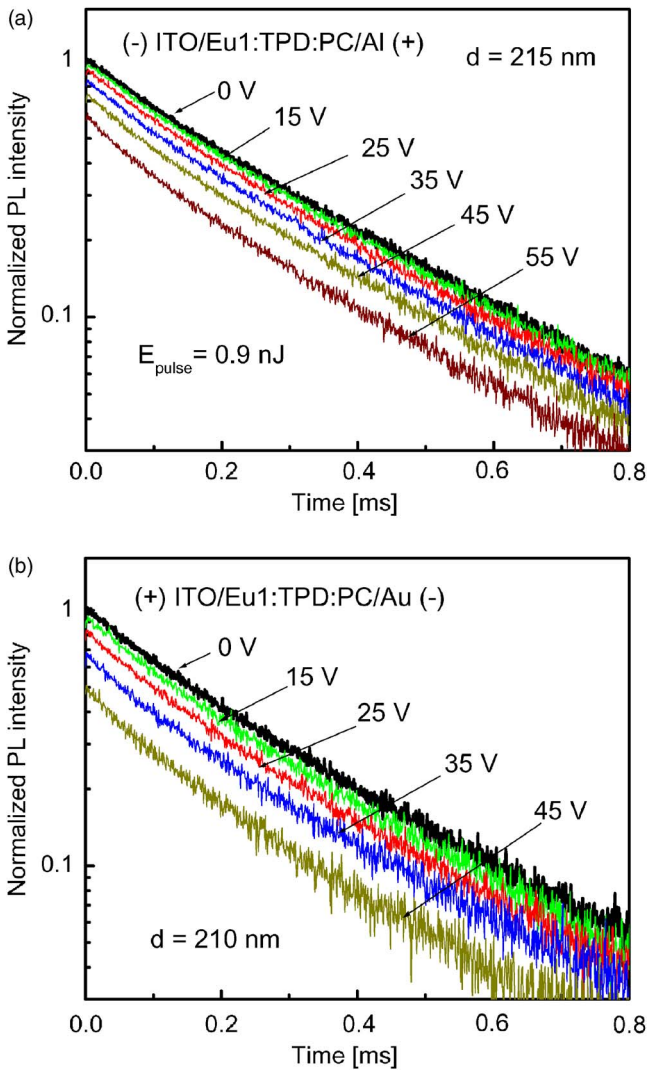

FIG. 5. (Color online) Time-resolved luminescence (λ_{em}=612 nm) for different voltages applied to the negatively (ITO^-) (a) and positively (ITO^+) (b) biased ITO layer Eul-doped (TPD:PC) blend structures as indicated in the figure. Excitation at wavelength λ_{exc}=355 nm, and the average quantal flux $I_0 = 8 \times 10^{13}$ photons/cm^2 s.

excitation light intensity [Fig. 4(b)]. We note that the long PL lifetimes of 480 μs arise because the *f*-shell transitions (see the electronic transitions scheme in Sec. IV A) are parity forbidden.[22]

Figure 5 shows the luminescence decay curves for Eu1-doped TPD:PC blend films under varying voltage applied to negatively or positively biased ITO electrode with the counterelectrical contacts Al^+ and Au^-, respectively. For both electrode combinations a significant reduction in the initial amplitude is observed while the curvature of the respective decays shows insignificant changes relative to the zero electric field decay as the voltage increases. A stronger quenching is observed in a system with the hole injecting ITO^+ anode.

In order to examine amplitude versus decay rate changes, we will define the amplitude PL quenching,

$$\delta_{\text{amplitude}} = \frac{N(t=0,F=0) - N(t=0,F)}{N(t=0,F=0)}, \tag{2}$$

and integrated PL quenching,

$$\delta_{\text{total}} = \frac{\int_0^\infty N(t=0,F=0)f(t)dt - \int_0^\infty N(t=0,F)f(t,F)dt}{\int_0^\infty N(t=0,F=0)f(t)dt}, \tag{3}$$

where $N(t=0,F)$ is the concentration of the emissive excited states of Eu^{3+} ion at time $t=0$ and electric field varying from $F=0$ to $F=F$, and $f(t),(f(t,F))$ represent time evolution functions of the population of excited states in the absence and presence of an external electric field, respectively. These two PL quenching efficiencies as a function of the applied field are presented in Fig. 6. The $\delta_{\text{amplitude}}$ has been calculated based on the assumption that the concentration of the excited states $N(t=0,F)$ is proportional to the initial ($t=0$) amplitudes at varying electric fields, and δ_{total} determined from the area under the PL decay curves taken at different electric

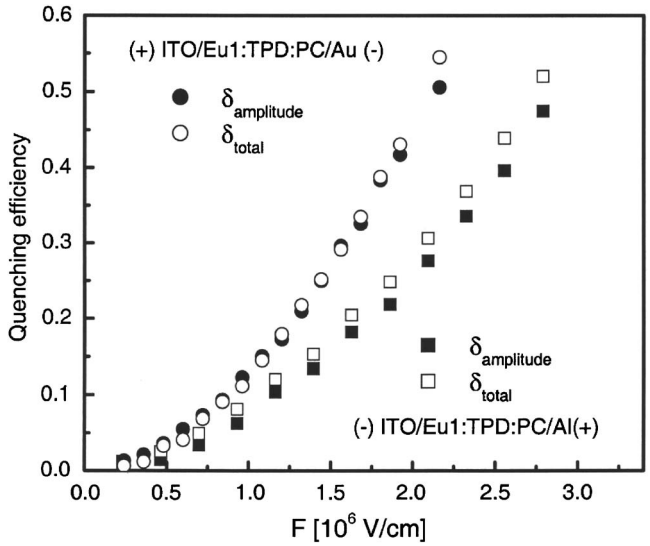

FIG. 6. Amplitude ($\delta_{\text{amplitude}}$) and integrated PL ($\delta_{\text{total}}$) quenching defined by Eqs. (2) and (3), respectively, as a function of electric field applied to ITO/Eul:TPD:PC/metal structures with positively (circles) and negatively (squares) biased ITO electrical contacts. These are the data summarizing the time-resolved experiments presented in Fig. 4.

fields for the samples as in Fig. 5. The quasi-identities of $\delta_{\text{amplitude}}$ and δ_{total} for the film structure with ITO^+ and slightly larger values of δ_{total} as compared with $\delta_{\text{amplitude}}$ for the film structure with the ITO^- cathode illustrate the effect of electric field on the decay rate, and suggest an additional channel for the decay of excited Eu^{3+} states, e.g., their field-assisted dissociation.

If the difference in the quenching effects for the structures with ITO^+ anode and ITO^- cathode is due to the space charge of holes injected from ITO^+ anode, electrical characteristics of these structures must be addressed. The dark current (i_{dark}) and current under illumination (i_{ph}) as a function of applied electric field for both film structures are shown in Fig. 7(a). From the figure it is clear that both are much greater (over three orders of magnitude) for the structure with the positively biased ITO electrode, confirming our supposition of much higher concentration of charge in the sample volume due to thermionic hole injection from ITO^+. Unlike for the structure with ITO^-, the current-field characteristics for the ITO^+ bias, except for the lowest applied fields, can well be approximated by the straight line plots of $\log(j/F^2)$ versus $F^{1/2}$ [Fig. 8(a)] that suggests the currents to be space-charge-limited currents (SCLCs), $j_{\text{SCLC}} = (9/8)\mu\varepsilon_0\varepsilon F^2/d$ (see, e.g., Ref. 1) with a field-dependent mobility $\mu \approx \mu_0 \exp(\beta_\mu F^{1/2})$, where μ_0 is the zero-field mobility and β_μ is the scaling factor of the $\mu(F)$ increase. Though the field-dependent mobility modifies the spatial distribution of charge and electric field within the sample, the SCL current density may still be well approximated by a Poole-Frenkel-type function,[23,24]

$$j \cong \frac{9}{8}\frac{\varepsilon_0\varepsilon\mu_0 F^2}{d}\exp(0.891\beta_\mu F^{1/2}). \quad (4)$$

The measured scaling factor of function (4) becomes then slightly lower than β_μ. Moreover and more important is that $j(F)$ dependence can preserve shape [Eq. (4)] even for non-

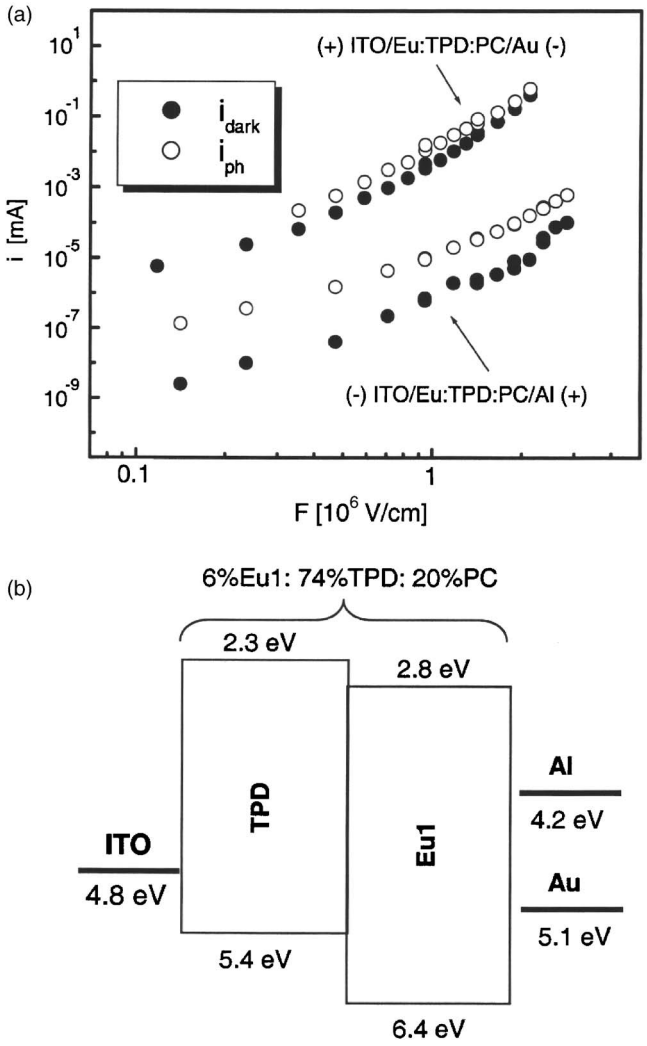

FIG. 7. Current-field characteristics (a) for the two respective structures from Fig. 5. A large increase in both dark (i_{dark})- and photocurrent (i_{ph}) can be seen when the ITO contact becomes positively biased. The energy level diagram for the materials used (b) explaining the observed asymmetry in the injection currents for the forward (ITO^+) and reversed (ITO^-) polarizations of the film structures.

Ohmic contacts limiting largely the current flow, $j(F) \approx (9/8)\varepsilon_0\varepsilon\mu_0^{\text{eff}}(F^2/d)\exp(\beta_\mu^{\text{eff}}F^{1/2})$ (Ref. 24). Its scaling factor β_μ^{eff} is then expected to exceed β_μ if the thermionic injection of charge obeys the one-dimensional (1D) Onsager-type mechanism described by a similar functional dependence $j_{\text{th}} = A_{\text{th}}F^{3/4}\exp(aF^{1/2})$ with $a = (e/kT) \times (e/4\pi\varepsilon_0\varepsilon)^{1/2}$ and A_{th} standing for a constant responsible for the primary carrier injection.[1] Such a behavior has been reported in experiment[25] and predicted by the calculations based on numerical methods.[24] The calculations have shown the scaling factor β_μ^{eff} and μ_0^{eff} to be dependent on the injection barrier height φ_{inj} above 0.3 eV. For example, $\beta_\mu^{\text{eff}}/\beta_\mu = 4.5$ and $\mu_0^{\text{eff}}/\mu_0 = 3 \times 10^{-3}$ for $\varphi_{\text{inj}} = 0.45$ eV. Since the hole injection barrier at the ITO^+/TPD interface $\varphi_{\text{inj}} \approx 0.5 \pm 0.1$ eV,[26] we expect β_μ^{eff} to substantially exceed β_μ, and μ_0 to be strongly reduced for our film structures, suggesting the current to be rather injection controlled than SCLC. Indeed, the 1D Onsager plot $\log(j_{\text{dark}}/F^{3/4})$ versus $F^{1/2}$ reproduces excellently the experimental data for

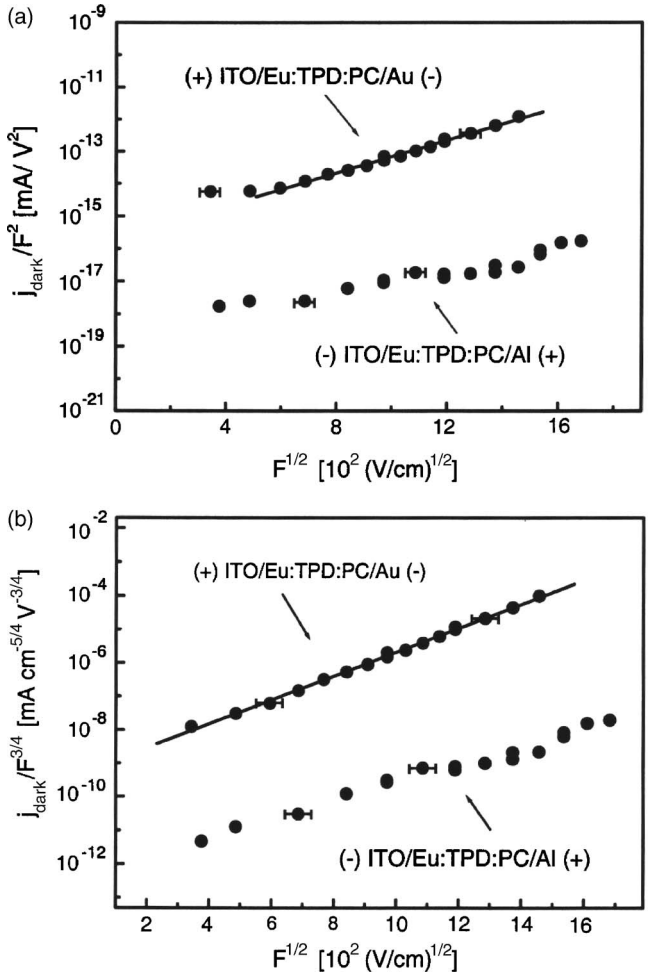

FIG. 8. Electric field dependencies of the currents from Fig. 6(a) in the $\log(j/F^2)$ vs $F^{1/2}$ representation based on the assumption the ITO$^+$ hole ($\mu_{\text{eff}}=\mu_h$) injection currents to flow under SCLC conditions (a), and in the $\log(j/F^{3/4})$ vs $F^{1/2}$ representation characteristic of the 1D Onsager model of charge separation at the ITO/emitter layer interface (b).

ITO$^+$-polarized structure, as can be seen from Fig. 8(b). The fit yields the thermionic injection parameters $A_{\text{th}}=6.0\times10^{-13}$ A cm$^{-5/4}$ V$^{-3/4}$, and $a=8.2\times10^{-3}$ (cm/V)$^{1/2}$ to be identified with its theoretical value calculated using a typical for organics, reasonable value of $\varepsilon=3.24$.

Here, a question arises what is the nature of the photocurrent. This point has been discussed in detail in our previous work,[12] showing the dark injection from ITO$^+$ to be enhanced by injection of electrons by the reaction of TPD singlet excitons on ITO$^-$ or Au$^-$ cathodes. By this, the single carrier (hole) injection current observed in the dark may become a much larger double injection current with different μ_{eff} and β_μ under sufficiently strong illumination as these quantities relate now to both holes and electrons. However, due to the small size of the illuminated spot and low average excitation intensity, the photocurrent for the samples studied in the present work only insignificantly exceeds the dark current (see Fig. 7) and, therefore, the photocurrent can be approximated by the motion of holes injected from the ITO$^+$ anode and generated by the dissociation in the sample bulk. In the ITO$^-$ case the photocurrent is relatively high and cannot be approximated by the dark current of the holes injected from Al$^+$ anode. The dark injection of holes from Al$^+$ is much weaker than that from the ITO$^+$ because of a large difference in the hole injection barrier to TPD hole transporting material, 0.6 eV for ITO$^+$ and 1.3 eV for Al$^+$ [see Fig. 7(b)]. The photocurrent is here most probably dominated by excitonic injection of electrons from ITO$^-$ cathode.

IV. ANALYSIS OF RESULTS AND DISCUSSION

A. Field versus charge quenching

When an Eu complex-doped layer is exposed to photons ($h\nu_{\text{exc}}$) exciting predominantly its matrix component (here TPD), Eu^{3+} ions are excited indirectly according to the scheme shown in Fig. 9. Their initial concentration can be defined as

$$N(t=0,F)=\frac{0.63E_{\text{pulse}}}{V_{\text{exc}}h\nu_{\text{exc}}}\varphi_{\text{tr}}^{(\text{HL})}\varphi_{\text{tr}}^{(\text{LC})}, \tag{5}$$

where E_{pulse} is the energy of individual light pulses, V_{exc} is the volume of the excited part of the sample, and $\varphi_{\text{tr}}^{(\text{HL})}$ and $\varphi_{\text{tr}}^{(\text{LC})}$ stand for the energy transfer efficiencies from TPD host to ligand (HL) and ligand to center (LC) (Eu^{3+}), respectively. In general, both of them are functions of the electric field applied and charge carrier concentration injected into the sample. These make $N(t=0,F)$ to change with field in a complex manner difficult to compare with experiment. However, due to a weak field dependence of some of the rate constants given in the scheme of Fig. 9, the field-dependent concentration of the excited Eu^{3+} ions may be approximated by (for explanations, see Appendix)

$$N(t=0,F)\cong\frac{0.63E_{\text{pulse}}}{V_{\text{exc}}h\nu_{\text{exc}}}\varphi_{\text{tr}}^{(\text{HL})}[1-\eta^{(\text{L})}(F)]\times\frac{k_{\text{tr}}^{(\text{LC})}}{\tau_{S,T}^{-1}+\gamma(F)n(F)}. \tag{6}$$

Here, $\varphi_{\text{tr}}^{(\text{HL})}(F)\cong$const has been assumed due to a weak field dependence of S_H^* dissociation rate constant $[k_d^{(\text{H})}]$ leading to less than 1% modulation of the TPD fluorescence component in the spectrum of the Eu^{3+}-doped films.[12] In Eq. (6) the field dependence of $\varphi_{\text{tr}}^{(\text{LC})}$ from Eq. (5) occurs through the field-dependent dissociation rate constant $[k_d^{(\text{L})}]$ of ligand triplet precursors singlet states $S_1^{(\text{L})}$ expressed by their dissociation efficiency $\eta^{(\text{L})}(F)=\mathbf{k}_d^{(^1\text{L})}/[\mathbf{k}_n^{(\text{L})}+\mathbf{k}_d^{(^1\text{L})}+\mathbf{k}_{\text{tr}}^{(^1\text{LC})}+\mathbf{k}_{\text{ISC}}^{(\text{L})}]$, the field-increasing concentration of injected charge $n(F)$ and generally field-dependent bimolecular ligand exciton–charge carrier interaction rate constant $\gamma(F)$. The quantity $\tau_{S,T}$ in Eq. (6) represents either the excited singlet or triplet intrinsic lifetime being by definition independent of electric field, $\tau_S(F)=[k_{\text{ISC}}^{(\text{L})}+k_{\text{tr}}^{(^1\text{LC})}]^{-1}=$const and $\tau_T(F)=[k_n^{(^3\text{L})}+k_{\text{tr}}^{(^3\text{LC})}]^{-1}=$const. An additional field-induced reduction in the decay time may be expected at the highest accessible fields allowing $^5D_0$ states to dissociate with a field-dependent rate constant $k_d^{(C)}$. More specifically, the excited Eu^{3+} ion imposes an electron transfer to or from the ligand, i.e., produces an intramolecular nonemissive charge-transfer (CT) state. The intramolecular recombination of the charge pair can regenerate the metal-located excited state. The charge transfer and re-

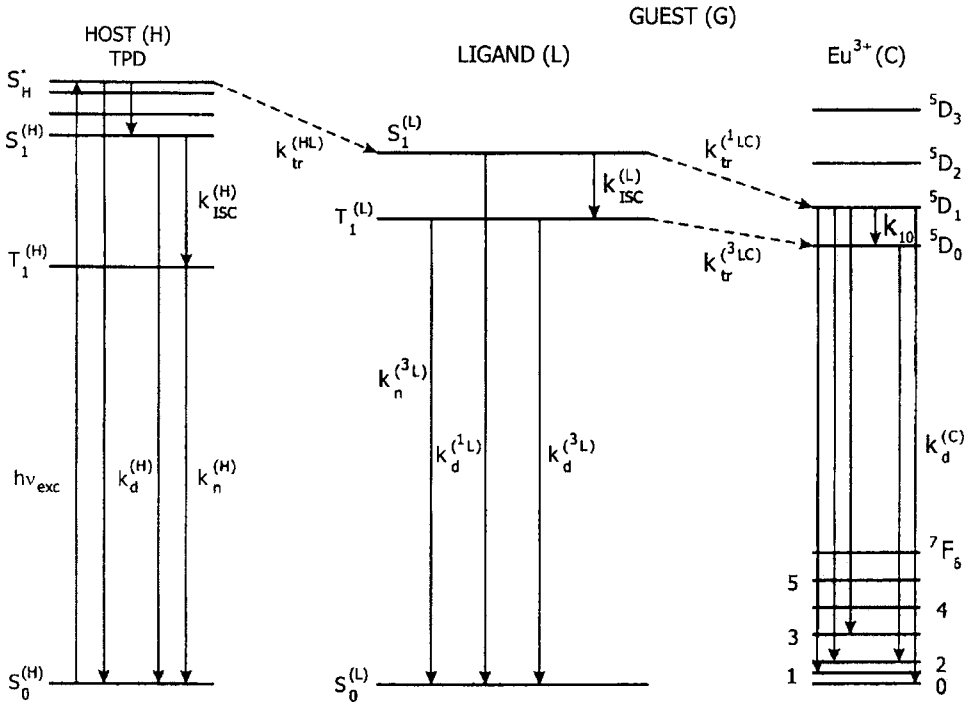

FIG. 9. Energy level diagram showing the energy transfer pathways in Eul complex-doped (TPD:PC) blends. For details see text.

combination rates define the equilibrium rate constant which at sufficiently high electric fields shifts the equilibrium toward CT states. Consequently, a drop in the $(Eu^{3+})^*$ emission lifetime could be expected. A slight reduction in the PL decay time at the highest applied voltages might be due to this effect (Fig. 5).

Referring back to Eq. (2) and substituting to it $N(t=0,F=0)$ and $N(t=0,F)$ resulting from Eq. (6) for $F=0$ and $F=F$, respectively, yields the overall (field and charge) quenching efficiency

$$\delta = \frac{\eta^{(L)}(F) + \gamma(F)n(F)\tau_{S,T}}{1 + \gamma(F)n(F)\tau_{S,T}}. \tag{7}$$

From Eq. (7) two characteristic approximations can be distinguished: (i) no exciton-charge carrier interaction $[n(F) \to 0]$, $\delta = \delta_{\text{dis}} = \eta^{(L)}(F)$, the field effect on luminescence being dominated by ligand excited states dissociation, and (ii) weak exciton-charge carrier interaction $[\gamma(F)n(F)\tau_{S,T} \ll 1]$, $\delta \approx \delta_{\text{dis}} + \delta_q$, where $\delta_q = \gamma(F)n(F)\tau_{S,T}$, the overall quenching stands here for a simple sum of pure field (δ_{dis}) and charge carrier $[\delta_q(n)]$ effect on luminescence, and $\delta \approx \delta_q$ if $\delta_{\text{dis}} \ll \delta_q$. In the latter case the annihilation of ligand excited states on charge carriers dominates the luminescence quenching process. For large and comparable modulation effects, the field- and charge-induced components are interrelated through the overall quenching efficiency as follows:

$$\delta = \delta_{\text{overall}} = \frac{\delta_{\text{dis}} + \delta_q}{1 + \delta_q}. \tag{8}$$

B. Electric field–assisted dissociation

The $\delta(F)$ behavior for (–)ITO/Eu1:TPD:PC/Al(+) film structure (Fig. 6) can be identified with case (i) since its low current (photocurrent)-field characteristic (Fig. 7) proves no significant space charge operating in the sample. One would expect $\delta(F) \approx \delta_{\text{dis}}(F)$ to follow a field-assisted dissociation mechanism to be responsible for the shape of the function $\delta_{\text{dis}}(F)$. As shown in Fig. 10, the three-dimensional (3D) Onsager model of geminate recombination[27] (for a more recent description of the model, see, e.g., Ref. 20) can successfully reproduce the amplitude PL quenching signal versus applied field. This model assumes the excited state [here $S_1^{(L)}$, see Fig. 9] to form a geminate Coulombically correlated electron-hole pair with a field-independent initial efficiency η_0 and initial separation distance r_0. Then, it can either recombine or dissociate in the diffusion process occurring in the carrier Coulombic field being modified by the applied external field. The fit to experimental data has been obtained following the Onsager expression for the geminate charge pair dissociation efficiency,

$$\eta(F) = \eta_0 \cdot \Omega(F) = \eta_0 \left[1 - \zeta^{-1} \sum_{l=0}^{\infty} P_j(r_c/r_0) P_j(\zeta) \right], \tag{9}$$

where

$$P_j(x) = P_{j-1}(x) - x^j \exp(-x)/j,$$

$$P_0(x) = 1 - \exp(-x), \tag{10}$$

and

$$r_c = \frac{e^2}{4\pi\varepsilon_0\varepsilon kT}, \tag{11}$$

$$\zeta = e r_0 |F| / kT. \tag{12}$$

Equation (11) defines the so-called Onsager radius—the intercarrier distance in charge pair, where the Coulombian attraction energy equals the thermal energy kT. Typically, it amounts to 18–20 nm with the dielectric constant $\varepsilon = 3-4$ at room temperature. Using this value and Onsager fitting parameters from Fig. 10(a), $\eta_0 = 1.0$ and $r_0/r_c = 0.09$, we arrive

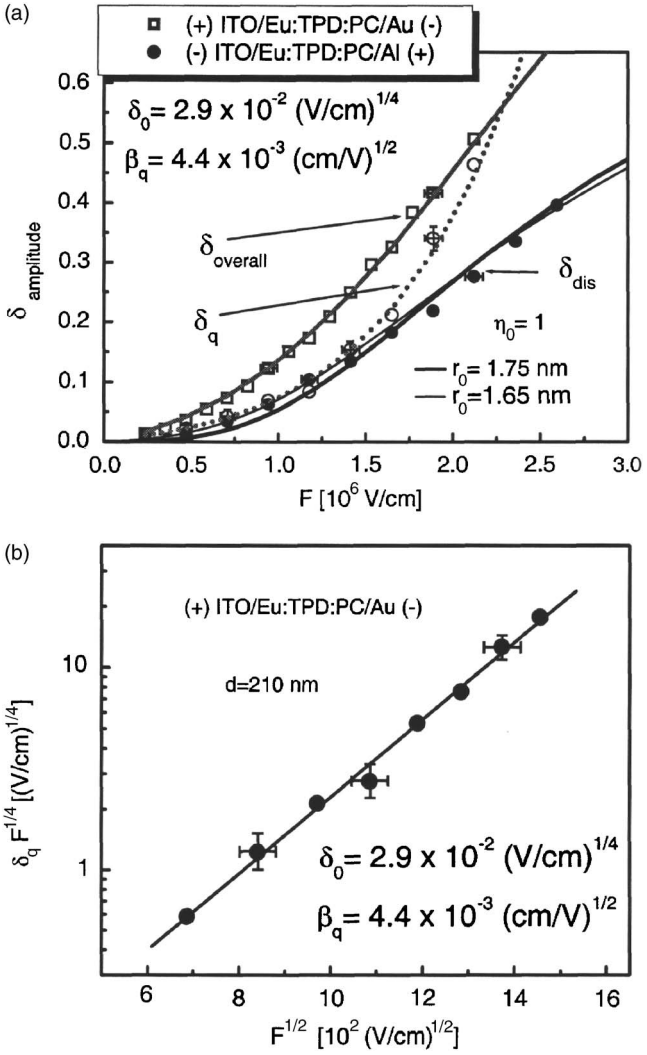

FIG. 10. (a) Amplitude luminescence quenching as a function of electric field applied the ITO^+- and ITO^--biased samples. Figure points are the present work experimental data, lines are theoretical fits according to Eq. (7). The δ_{dis} fits the 3D Onsager theory according to Eq. (7) with $n(x)=0$, identified with Eq. (9), and combined dissociation and exciton-charge carrier annihilation ($\delta_{overall}$ according to Eq. (8) including $\delta_{dis}=\eta^{(L)}$ [Eq. (9)] and δ_q [Eq. (13)]. Two Onsager fits are presented for $F=U/d$ (nominal electric field) (thick solid line) and for $F_{eff}=F+F_i$ in the presence of an internal field $F_i=2.8\times10^5$ V/cm (thin solid line). (b) The straight line charge quenching plot $\log(\delta_q F^{1/4})$ vs $F^{1/2}$ illustrating the effect to be underlain by the charge injected according to the 1D Onsager model represented by Eq. (13).

at $r_0=1.75$ nm. This result may change if an electron space charge creating an internal electric field (F_i) is present in the sample. Such a field (on a 10^5 V/cm level) as a rule appears in organic photoconducting films due to the photogeneration of charge.[28] Indeed, the fitting procedure, using an effective electric field $F_{eff}=F+F_i$ with $F_i=2.8\times10^5$ V/cm, yields a better fit (especially in the low-field region) reducing r_0 to 1.65 nm [thin solid line in Fig. 10(a)]. The high values of both η_0 and r_0 suggest the dissociating state to be relatively weakly bound supporting its designation as the excited ligand singlet, $S_1^{(L)}$. The overall depopulation rate of state $S_1^{(L)}$ includes the intersystem crossing to the ligand triplet $T_1^{(L)}$ and energy transfer to the Eu^{3+} ion $^5D_1$ state: $k_{S_1}^{(L)}=k_{ISC}^{(L)}+k_{tr}^{(LC)}$. On the microsecond scale (Fig. 11), the rise time of the $^5D_0\rightarrow{}^7F_2$ luminescence observed at 612 nm can be established. The final PL level is reached after approximately 0.8–1.0 μs independent of the sample composition. This rise time correlates well with that found for europium thenoyltrifluoroacetonate [$Eu(tta)_3$] complex in solution,[29] showing to be an inherent feature of the Eu^{3+} ion. In fact, based on its correlation with the measured decays of the $^5D_1\rightarrow{}^7F_{1-3}$ luminescence signals, the rise time has been attributed to the intraion transitions between states $^5D_1$ and $^5D_0$ (in Fig. 8 indicated by the rate constant k_{10}).[29]

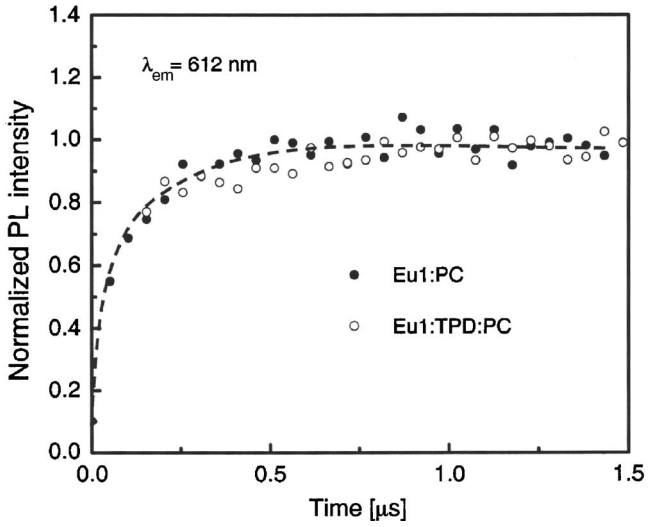

FIG. 11. The rise part of the kinetic curve for time-resolved luminescence of Eul-doped (TPD:PC) blend and Eul-doped PC films detected at 612 nm with excitation wavelength of 355 nm. The dashed line is a guide to the eyes.

To weaken the role of the field-enhanced dissociation in the total electric field–induced modulation of the time resolved luminescence (EML), phosphors with strongly bound singlet excitons on their ligands are required, leading to a reduction in the Onsager parameters η_0 and r_0. One of the ways to reach this goal would be the synthesis of phosphor complexes with a stronger coupling between ligand and central ion. The rate constant $k_{tr}^{(1LC)}$ may then become more effectively competing with the dissociation rate constant $k_d^{(1L)}$, leading to a decrease in the luminescence quenching. Another possibility is to replace the hole transporting material with a compound of a lower ionization potential that would reduce $k_d^{(1L)}$.

C. Quenching by injected charge

The observation of increased PL quenching for the structure with the positively biased ITO electrode, ITO^+ (Fig. 6), indicates a new quenching mechanism to operate in addition to the dissociation of excited states responsible for the EML in the structure with the ITO cathode (ITO^-). We propose that the additional channel for the EML is due to the annihilation of ligand singlets and/or triplets on the injected charge, as already mentioned above. The charge quenching component of the EML should thus by definition follow the field dependence of the charge concentration, $n(F)=j(F)/e\mu F$, which, using Eq. (4) and its injection-modified version discussed afterward, can be expressed as

$$\delta_q = \gamma n(F)\tau_{S,T} \cong \frac{\gamma\tau_{S,T}A_{\text{th}}}{e\mu_0 F^{1/4}} \exp[(a-\beta_u)F^{1/2}]. \quad (13)$$

As discussed previously,[12] the charge-induced PL quenching component (δ_q) can be positive, increasing monotonously with the applied voltage, or tending to a saturation value and ending on a roll off at high electric fields ($>10^6$ V/cm) as was the case with Eul. Negative values ($\delta_q<0$) have also been observed.[11,12] The $\delta_q(F)$ decrease has been attributed to the electron space charge generated by excitonic reactions at the ITO^- and Au^- cathodes. Its recombination with the space charge of holes injected at Au^+ and ITO^+ respective anodes produces an additional to the photoexcited exciton population of emissive states, diminishing the overall PL quenching signal δ_{overall}. By definition, the degree of its reduction depends on the electron concentration and is expected to increase with light excitation intensity and the optically excited volume of the sample. Since both are here much lower than those used previously, it is not surprising that the values of δ_{overall}, reaching 50% (see Fig. 6), exceed by a factor of 2, the maximum δ_{overall} reported in Refs. 11 and 12. Moreover, a monotonic field increase of the δ_q is here observed instead of its saturation or decrease.

The experimental dependence of $\delta_q(F)$ can be extracted from the experimental curves of $\delta_{\text{dis}}(F)$ and $\delta(F)$, presented in Fig. 6, employing Eq. (8). The result is shown in Fig. 10(b). The $\delta_q(F)$ follows a straight line plot of $\log[\delta_q(F)\times F^{1/4}]$ versus $F^{1/2}$ showing a supralinear 1D Onsager-type function increase of δ_q with field, as predicted by Eq. (13) [see Fig. 10(a)]. From the fit $\delta_0=\gamma A_{\text{th}}\tau_{S,T}/e\mu_0=2.9\times10^{-2}$ $(\text{V/cm})^{1/4}$ and $\beta_q=a-\beta_\mu=4.4\times10^{-3}$ $(\text{cm/V})^{1/2}$ follow. Furthermore, having A_{th} and the product of $\gamma\tau_{S,T}$, μ_0 can be calculated and $\mu(F)=\mu_0\exp(\beta_\mu F^{1/2})$ obtained with $\beta_\mu=a-\beta_q=3.8\times10^{-3}$ $(\text{cm/V})^{1/2}$. It is possible to calculate $\gamma\tau_{S,T}$ from the definition equation for $\delta_q(F)=\gamma\tau_{S,T}n(F)$ assuming the high field current to enter the SCLC regime and thus $n(F)=n_{\text{SCLC}}(F)=(3/2)\varepsilon_0\varepsilon F/ed$ ($\varepsilon=3.24$). For $F_{\max}=2.12\times10^6$ V/cm, $\delta_q(F_{\max})=0.47$, $n(F_{\max})=2.7\times10^{17}$ cm^{-3}, and $\gamma\tau_{S,T}=1.74\times10^{-18}$ cm^3. Using this $\gamma\tau_{S,T}$ product value, we arrive at $\mu_0=2.2\times10^{-10}$ $\text{cm}^2/\text{V s}$ and, consequently, $\mu(F_{\max})\approx5.56\times10^{-8}$ $\text{cm}^2/\text{V s}$. In turn, $n(F_{\max})\approx j_{\max}/e\mu(F_{\max})F_{\max}\approx2.9\times10^{17}$ cm^{-3} (with $j_{\max}=5.43$ mA/cm^2) is consistent with $n_{\text{SCLC}}(F_{\max})$, proving the correctness of the assumption $n(F)=n_{\text{SCLC}}(F)$ at electric fields above 2×10^6 V/cm. The ligand exciton-charge carrier interaction rate constant results from the value $\gamma\tau_{S,T}$ inferred from experiment and is related to the lifetime of either singlet or triplet excited ligand states, $\gamma=1.74\times10^{-18}$ $\text{cm}^3/\tau_{S,T}$. A short lifetime $\tau_{S,T}$ would lead to a high value of the interaction constant γ. Reported values of τ_S vary from 1.7 ns, for the free ligand,[30] through ≈1 ns for its weak coupling to triplets,[29] down to 42 ps for the strong singlet-triplet coupling ($k_{\text{ISC}}=2.4\times10^{10}$ s^{-1}).[31] This produces a γ span, $\gamma_{sq}=1\times10^{-9}/4\times10^{-8}$ cm^3/s. The long-living triplets, though can interact efficiently with charge carriers, have been shown to be inactive in the energy transfer to emissive ion Eu^{3+} (Ref. 29), thus they do not contribute to the observed quenching effects.

Interaction in a bimolecular reaction of ligand singlet, $S_1^{(L)}$, with a TPD-transported hole, TPD^+, is described by a second order rate constant,[1,20]

$$\gamma_{sq} = 4\pi R_c(D_S + D_h) \quad (14)$$

expressed by the exciton capture distance R_c (quenching distance between the particles), and the diffusion coefficients of singlet, D_S, and hole, D_h, respectively. Even with the highest attainable $D_h=\mu(F_{\max})kT/e\approx1.4\times10^{-9}$ cm^2/s, the contribution of the carrier motion to γ_{sq} is negligible since $4\pi R_c D_h\approx2\times10^{-15}$ cm^3/s falls six orders of magnitude below the lower limit of $\gamma_{sq}=10^{-9}$ cm^3/s here evaluated. In the calculation, the carrier hopping distance $R_c\approx1$ nm was taken and the applicability of Einstein's relation between D_h and μ assumed. Consequently, Eq. (14) simplifies to

$$\gamma_{sq} = 4\pi R_{\text{eff}} D_S, \quad (15)$$

where, generally, R_{eff} takes into account the long-distance (Förster type) energy transfer from the excited ligand singlet to the TPD located hole (TPD^+),[1,32]

$$R_{\text{eff}} = R_c + 0.724\left(\frac{R_0^6}{\tau_S D_S}\right)^{1/4}. \quad (16)$$

For a given γ_{sq} the relation between D_S and Förster radius R_0 can be extracted from Eqs. (15) and (16). It is shown in Fig. 12(a) along with the plot of the expression,[1,33]

$$\gamma_{sq} = 4\pi\frac{\Gamma(3/4)}{\Gamma(5/4)}\frac{D_S^{3/4}R_0^{3/2}}{\tau_S^{1/4}}, \quad (17)$$

representing the energy transfer $S\rightarrow TPD^+$ when the Förster mechanism dominates $[(R_0/R_c)/\tau_S \gg 6D_S/R_c^2]$. Here, Γ is the function gamma. From Fig. 12(a) it is clear that except for small values of R_0 (<2 nm), the transfer is dominated by the long-range capture mechanism, the diffusion length of excitons $l_S=\sqrt{6D_S\tau_S}<0.7R_0(R_0/R_c)^2$. Typically, for $R_0=3$ nm and $R_c=1$ nm, $l_S<19$ nm which corresponds to $D_S=3.5\times10^{-4}$ cm^2/s and $D_S=10^{-2}$ cm^2/s for the above mentioned respective limits of the singlet lifetime. While the second value is very high and hardly conceivable in amorphous films, the first one reasonably exceeds $D_S=3\times10^{-5}$ cm^2/s obtained previously for a 6% Ir complex phosphor-doped TPD:PC blends.[13] This difference, related to the low value of the γ_{sq} $[=(2\pm1)\times10^{-11}$ $\text{cm}^3/\text{s}]$, reflects the difference in the quenching mechanism shown to be associated with the diffusivity of excited singlets of TPD rather than that of the Ir complex. The relation between γ_{sq} and D_S of the excited ligand is presented in Fig. 12(b), as a determined from Eq. (15) for two limiting values of the singlet exciton lifetime. Apparently, two regions of D_S can be distinguished. For its low values ($<10^{-4}$ cm^2/s) the Förster-type transfer is dominating, $\gamma_{sq}\sim D_S^{3/4}$, for large values of D_S, the γ_{sq} is dominated by the exciton hopping with $\gamma_{sq}\sim D_S$. In our PL quenching measurements, γ_{sq} is determined between 1.4×10^{-9} cm^3/s with $\tau_S=1.7$ ns and 4×10^{-8} cm^3/s with $\tau_S=42$ ps. These values fall in the range, where both mechanisms give comparable contributions to γ_{sq}, the $\gamma_{sq}(D_S)$ deviates from either 3/4 and 1 power function of D_S.

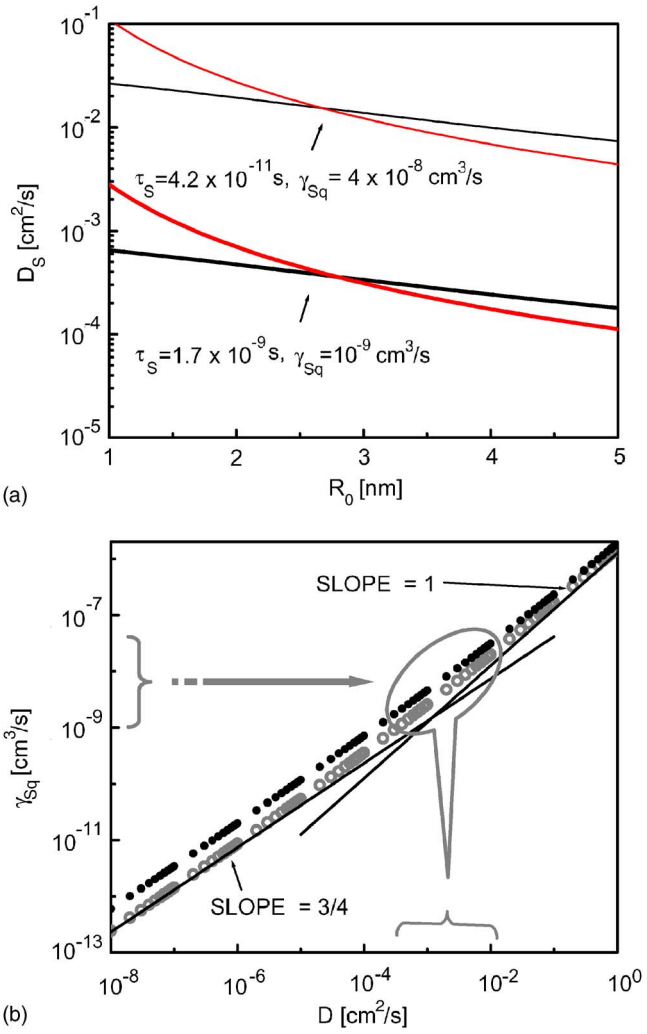

FIG. 12. (Color online) Interrelations between various energy transfer parameters from excited ligand singlets to TPD-located holes: (a) the singlet exciton diffusion coefficient for varying Förster radius R_0 at two given limits of exciton-charge carrier interaction rate constants (γ_{Sq}) as calculated from Eqs. (15) and (16) (straight lines), and approximated by Eq. (17) (solid curves), (b) γ_{Sq} at varying D_S for two different exciton lifetimes τ_S =1.7 ns (open circles) and τ_S=42 ps (full circles); the region appropriate to the data of the present work is indicated by an elliptic form border. The plot data obtained from Eqs. (15) and (16) with R_c=1 nm and R_0=3 nm.

In Fig. 13 the contribution of δ_q to the sum of charge and dissociation quenching $[\Delta_q = \delta_q/(\delta_q + \delta_{\text{dis}})]$ is shown as a function of electric field in comparison to the relative contribution (Δ_{dis}) of δ_{dis}. The minimum of Δ_q naturally corresponds to the maximum of Δ_{dis} at a field of 10^6 V/cm. This nonmonotonous behavior reflects different shapes of functions $\delta_{\text{dis}}(F)$ [Eq. (9)] and δ_q [Eq. (13)]. While $\delta_q(F)$ increases monotonously with field, δ_{dis} tends to saturation at very high fields [cf. Fig. 10(a)], leading to weakening of the role of dissociation quenching for δ_{total}. A good agreement between theoretical predictions (solid lines) and experimental data (circles) confirms that underlying dependencies of the charge and dissociation quenching on applied electric field are correctly described by this paper. From Fig. 13 it is also seen that SCLC conditions shift the two extremes toward higher fields and increase the role of the charge quenching as might be the situation in organic LEDs with

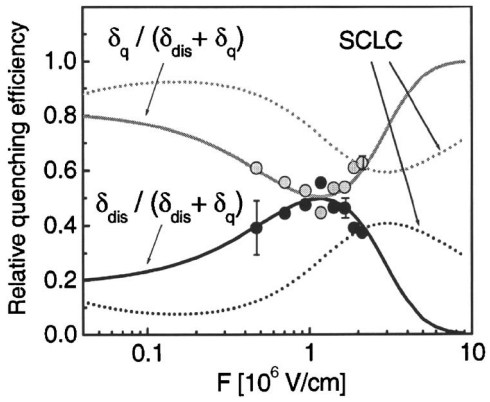

FIG. 13. The relative changes of the charge (δ_q) and dissociation (δ_{dis}) quenching with the applied electric field (circles). The solid curves represent theoretical predictions using Eqs. (9) and (13), and they demonstrate good agreement with the behavior expected for dissociation and charge quenching. Parameters extracted from Fig. 9 are used to obtain the curves. The 1D Onsager fit for the δ_{dis} in the presence of the internal field has been employed in the calculations. The dotted curves are predictions of the above relative changes under SCLC conditions.

Ohmic injecting contacts. Nevertheless, the dissociation is still an important process constituting almost 40% of the total quenching effects at a very high field of 3×10^6 V/cm.

V. CONCLUSIONS

The present work undertakes one of the most significant problems facing the electrophosphorescent devices that is the high field roll off in their quantum efficiency. The luminescence at varying electric fields has been examined in an important class of emitters employed in monochromatic organic LEDs, using successfully a time-resolved luminescence technique which allows us to identify the species that respond directly to the applied electric field. We found that electric field applied to thin film linelike emissive structures based on rare-earth organic complexes, provided with a charge injecting electrode, imposes annihilation of excited states by two different modes: (i) the electric field–enhanced dissociation and (ii) the interaction with the field-controlled concentration of injected charge carriers. The present work time-resolved electric field–induced luminescence quenching measurements and their analysis allow us to prove that unlike luminescence of some other organic films (e.g., phthalocyanines), the Eu^{3+} ion emission from Eu complex-doped blend films exhibits dominating amplitude quenching with only residual modulation of its lifetime. The amplitude quenching indicates the existence of precursor states of the emissive $^5D_0$ state of the Eu^{3+} ion, and these are excited states of the organic ligand and higher ^5D_n states preceding the emissive state that experience a decay imposed by the above two quenching mechanisms. A satisfactory description of the dissociation quenching component is given applying the classical 3D Onsager model allowing the initial separation distance of the electron-hole pairs to be evaluated on r_0 =1.65 nm. Another important conclusion is that the exciton-charge carrier annihilation is largely controlled by the long-range energy transfer of singlet ligand excitons, acting as precursors to the emissive Eu^{3+} states, to the host material-located charge carriers. Such a quenching process can ac-

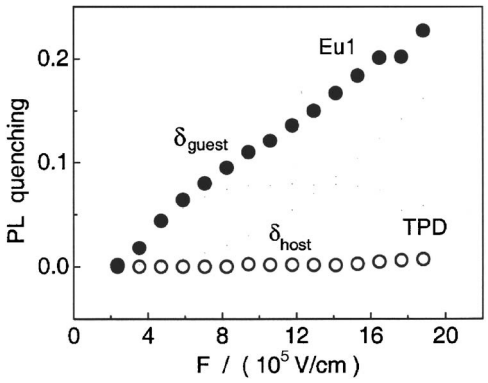

FIG. 14. The guest (Eul) and host (TPD) PL quenching from $h\nu \rightarrow \mathrm{ITO}^{+}/6$ wt % Eul:74 wt % TPD:20 wt % PC (70–100 nm)/Au^{-} film structures at varying steady-state electric field F. The data have been obtained at excitation wavelength $\lambda_{exc}=350$ nm and intensity $I_0=7\times10^{14}$ quanta/cm^2 s. The emission recorded at 610 nm (guest) and 420 nm (host).

count for the large current densities emission efficiency roll off observed in other organic LED emitters. To reduce the annihilation efficiency of excited ligand states, a system may incorporate rare-earth complexes weakly coupled to charged molecules of the matrix, revealing on their ligand enhanced singlet-triplet intersystem crossing and triplet energy transfer to the central metal ion.

ACKNOWLEDGMENTS

This work was supported by funds from the MURST (FIRB Project RBNE03S7XZ "SYNERGY"), the CARIPLO Foundation, and the RTN-EUROFET (Project No. HPRN-CT-2002-00327). The contribution from Dr. M. Cocchi and Dr. D. Virgili was supported by funds of CNR Project No. PM-P04-010 (MACOL) and by the FIRB projects "LUCI" and "NODIS."

APPENDIX: TPD HOST FLUORESCENCE QUENCHING

Equation (6) stands for an approximation of a more complex equation that, in principle, should include the field-enhanced dissociation of ^3L and S_H^* and interactions of these excited species with charge carriers. However, it has been shown that the efficient sensitization of the Eu^{3+} emission takes place through singlet pathway[29] that is $k_{tr}^{(^1\mathrm{LC})} \gg k_{tr}^{(^3\mathrm{LC})}$ (cf. Fig. 9). Thus, ^3L, even if quenched by dissociation and/or by charge carriers, would not contribute to the quenching of the emissive Eu^{3+} states. In order to evaluate the contribution to the overall quenching of S_H^* host excited states, we have performed a steady-state electric field quenching study of the Eu:TPD:PC samples, recording at the same time the emission of the Eu guest ($\lambda_{em}=610$ nm) and TPD host ($\lambda_{em}=420$ nm). The results are shown in Fig. 14.

We note that due to the electrical contact bias ($\mathrm{ITO}^{+}/\mathrm{Au}^{-}$), the PL quenching contains both dissociation and charge carrier quenching components. A large difference in the quenching of the guest and host emission is obvious. The host quenching component contributing to the total quenching signal can safely be neglected. This experimental observation suggests that a fast electron transfer from the excited TPD S_H^* state to more electronegative Eul molecule [see Fig. 7(b)] takes place, forming a geminate heterocharge transfer state (CT) (charge-transfer exciplex: $\mathrm{TPD}^{+}\mathrm{Eu1}^{-}$) with a field independent probability η_0. The geminate pair at a separation distance r_0 either dissociates thermally into free carriers with the electric field-dependent probability $\Omega(F)$ or recombines to give excited complex ligands, ^1L, ^3L. By this the dissociation process only insignificantly reduces the population of S_H^* and becomes rather an additional pathway to produce the excited ligands. A weak quenching of S_H^* states by holes located at TPD^{+} seems to be a simple consequence of the fast electron transfer from S_H^* to Eul. These suppositions do not exclude other possible reasons of weak quenching of the excited singlets of TPD as, for example, fast radiationless deactivation of hot S_H^* states to lower excited states including the ground state. In view of the presented properties of the excited states ^3L and S_H^*, it is justified to consider the amplitude quenching effect on the Eu^{3+} emission as a result largely dominated by the dissociation and interaction with TPD^{+} ions of its singlet ligand precursor ^1L, and, thus, Eq. (6) to be treated as an appropriate approximation for the concentration of the excited Eu^{3+} states.

[1] J. Kalinowski, *Organic Light Emitting Diodes: Principles, Characteristics, and Processes* (Dekker, New York, 2005).
[2] G. E. Jabbour, J.-F. Wang, B. Kippelen, and N. Peyghambarian, Jpn. J. Appl. Phys., Part 2 **38**, L1553 (1999).
[3] J. Kalinowski, W. Stampor, M. Cocchi, D. Virgili, and V. Fattori, Appl. Phys. Lett. **86**, 241106 (2005).
[4] M. A. Baldo, C. Adachi, and S. R. Forrest, Phys. Rev. B **62**, 10967 (2000).
[5] Z. Hong, C. Liang, R. Li, D. Zhao, D. Fan, D. Wang, B. Chu, F. Zang, L.-S. Hong, and S.-T. Lee, Adv. Mater. (Weinheim, Ger.) **13**, 1241 (2001).
[6] C. Adachi, M. A. Baldo, and S. R. Forrest, J. Appl. Phys. **87**, 8049 (2000).
[7] J. Kalinowski, W. Stampor, J. Mężyk, M. Cocchi, D. Virgili, V. Fattori, and P. Di Marco, Phys. Rev. B **66**, 235321 (2002).
[8] J. Mężyk, J. Kalinowski, F. Meinardi, and R. Tubino, Chem. Phys. Lett. **395**, 321 (2004).
[9] J. Mężyk, J. Kalinowski, F. Meinardi, and R. Tubino, Appl. Phys. Lett. **86**, 111916 (2005).
[10] J. Kalinowski, J. Mężyk, F. Meinardi, R. Tubino, M. Cocchi, and D. Virgili, J. Appl. Phys. **98**, 063532 (2005).
[11] D. Virgili, M. Cocchi, V. Fattori, J. Kalinowski, and W. Stampor, Appl. Phys. Lett. **88**, 051102 (2006).
[12] J. Kalinowski, W. Stampor, M. Cocchi, D. Virgili, and V. Fattori, J. Appl. Phys. **100**, 034318 (2006).
[13] J. Kalinowski, W. Stampor, J. Szmytkowski, D. Virgili, M. Cocchi, V. Fattori, and C. Sabatini, Phys. Rev. B **74**, 085316 (2006).
[14] T. Li, H. Fukuyama, Y. Yamagata, H.-L. Lan, and J. Kido, Polym. Adv. Technol. **15**, 302 (2004).
[15] H.-G. Lin, Y.-I. Lee, S. Park, K. Jang, and S.-Su. Kim, J. Lumin. **110**, 11 (2004).
[16] O. L. Malta, H. F. Brito, J. E. S. Menezes, F. R. Gonçalves e Silva, C. de Mello Donegá, and S. Alves, Jr., Chem. Phys. Lett. **282**, 233 (1998).
[17] M. I. Khan, G. C. Bazan, and Z. D. Popovic, Chem. Phys. Lett. **298**, 309 (1998).
[18] L. Miozzo, A. Papagni, M. Cerminara, F. Meinardi, R. Tubino, and C. Botta, Chem. Phys. Lett. **399**, 152 (2004).
[19] M.-H. Lu and J. C. Sturm, J. Appl. Phys. **91**, 595 (2002).
[20] M. Pope and C. E. Swenberg, *Electronic Processes in Organic Crystals* (Clarendon, Oxford, 1982).
[21] J. Kalinowski, V. Fattori, and P. Di Marco, Chem. Phys. **266**, 85 (2001).
[22] A. P. B. Sinha, in *Spectroscopy in Inorganic Systems*, edited by C. N. R. Rao and J. R. Ferraro (Academic, New York, 1971), Vol. 2.
[23] P. N. Murgatroyd, J. Phys. D **3**, 151 (1970).
[24] G. G. Malliaras and J. C. Scott, J. Appl. Phys. **85**, 7426 (1999).

[25] J. Kalinowski, L. C. Picciolo, H. Murata, and Z. H. Kafafi, J. Appl. Phys. **89**, 1866 (2001).
[26] H. Antoniadis, J. N. Miller, D. B. Roitman, and I. H. Cambell, IEEE Trans. Electron Devices **44**, 1289 (1997).
[27] L. Onsager, Phys. Rev. **54**, 554 (1938).
[28] J. Kalinowski, W. Stampor, and P. Di Marco, J. Electrochem. Soc. **143**, 315 (1996).
[29] C. Yang, L.-M. Fu, J.-P. Zhang, W.-T. Wong, X.-C. Ai, Y.-F. Qiao, B.-s. Zou, and L.-L. Gui, Angew. Chem., Int. Ed. **43**, 5010 (2004).
[30] S. Quici, G. Marzanni, M. Cavazzini, P. L. Anelli, M. Botta, E. Gianolio, G. Accorsi, N. Armaroli, and F. Barigelletti, Inorg. Chem. **41**, 2777 (2002).
[31] H. Lemmetyinen, E. Vuorimaa, A. Jutila, V.-M. Mukkala, H. Takalo, and J. Kankare, Luminescence **15**, 341 (2000).
[32] U. Gösele, M. Hauser, U. K. A. Klein, and R. Frey, Chem. Phys. Lett. **34**, 519 (1975).
[33] V. A. Benderskii, V. Kh. Brikenshtein, A. G. Lavrushko, and P. G. Filippov, Phys. Status Solidi B **86**, 445 (1978).